Wearable Dual-Layer Planar Magnetoinductive Waveguide for Wireless Body Area Networks

Connor B. Jenkins, *Student Member, IEEE*, and Asimina Kiourti, *Senior Member, IEEE*

***Abstract*— We have previously reported wearable magnetoinductive waveguides (MIW) for wireless body area networks (WBANs) that significantly outperform the state-of-the-art in terms of path loss, data rate, interference, security, and more. MIWs placed in a planar way upon the human body are most promising but suffer from a large deterioration in performance under mechanical failures and clothing transitions (e.g., from 10.62 dB to 28.44 dB minimum loss and from 21% to 0.77% fractional bandwidth). In this work, we overcome both limitations via a novel dual-layer planar MIW design that utilizes two layers of resonant loops stacked upon each other. Concurrently, this design maintains all benefits of MIW-based WBANs and improves the link budget by >5 dB vs. our previous single-layer MIWs and by >60-70dB vs. state-of-the-art WBANs. We herewith report a theoretical model of dual-layer MIWs that relies on the dispersion relation and validate it both numerically and experimentally. We also discuss the improvements vs. our previously reported MIW designs and address design considerations, including electromagnetic safety. This work cements MIWs as a future technology to be used in low-loss WBANs for full body applications.**

***Index Terms*—Electrically small resonant loops, magnetoinductive waveguide (MIW), magnetoinductive waves (MI waves), wireless body area networks (WBANs).**

I. Introduction

WEARABLE TECHNOLOGY is growing with applications present in fields ranging from medicine to video games [1-5]. Soon, it will be possible to have complete wearable systems that connect multiple wireless nodes on the body. These nodes must be able to reliably communicate with one another and to any central processing unit. The communication networks that connect these devices are known as Wireless Body-Area Networks (WBANs).

Current technologies used to form WBANs include Radio Frequency (RF)[1, 2, 4-6], Human Body Communication (HBC) [7-10], Magnetic Induction (MI) [11, 12] and a variety of e-textile solutions including NFC enabled clothing [13-15], surface wave-based solutions [16], and flexible waveguides [17]. However, these suffer from either high path loss (RF, HBC, and MI) or practical considerations related to robustness and wearability (e-textile solutions) [18].

This work was supported by the National Science Foundation under Grant 2053318.

The authors are with the ElectroScience Laboratory, Department of Electrical and Computer Engineering, The Ohio State University, Columbus, OH 43212 USA (e-mail: jenkins.1124@osu.edu, kiourti.1@osu.edu)

TABLE I
COMPARISON OF MIW-BASED WBAN TECHNOLOGIES

	Axial MIW	Single-Layer Planar MIW	Dual-Layer Planar MIW (Proposed)
Path Loss	Very Low	Very Low	Extremely Low
Unobtrusive	Yes	Yes	Yes
Interference	Negligible	Negligible	Negligible
Security	High	High	High
Data Rate	High	High	Very High
Frequency Selection	Restricted	Flexible	Flexible
Full-Body Integration	No	Yes	Yes
Robustness to Mechanical Failures	High	Low	High
Clothing Transition Robustness	-	Low	High

To address these limitations in the state-of-the-art, we recently reported a new class of wearable magnetoinductive waveguides (MIWs) that can be placed either axially (axial design) or longitudinally (planar design) upon the human body [19, 18]. The MIWs are formed by taking electrically small conductive loops, loading them with a capacitor to achieve resonance at the desired frequency, and placing them in close proximity to each other. The transmit loop is first excited with a current, which in turn produces a magnetic field. Through Faraday's law of induction, this field produces current on the neighboring loops and this process continues until reaching the last loop thereby forming traveling magnetoinductive waves (MI waves). The axial design boasts a large improvement in link budget vs. the state-of-the-art (50-60 dB), is robust to limb motion, and mechanical failures. However, it cannot be scaled to all frequencies, and cannot be used across the entire human body due to the reliance on underlying anatomy. By contrast, the planar design maintains the abovementioned advantages of axial MIWs while also being scalable to any frequency and robust to curvature of human anatomy. However, it suffers from a large deterioration in performance under mechanical failures and clothing transitions (e.g., from 10.62 dB to 28.44 dB minimum loss and from 21% to 0.77% fractional bandwidth).

In this work, we take a major step forward and introduce a

TABLE II
COMPARISON OF SINGLE- AND DUAL-LAYER PLANAR MIW

		Single-Layer	Dual-Layer (Proposed)
Ideal Case	Min. Loss (dB)	10.34	4.25
	Bandwidth (MHz)	8.40	9.44
2 Broken Loops	Min. Loss (dB)	27.31	16.75
	Bandwidth (MHz)	0.96	7.04
Clothing Transition (Longitudinal)	Min. Loss (dB)	10.54	4.46
	Bandwidth (MHz)	5.20	7.96

novel dual-layer planar MIW that resolves the limitations of our previous single-layer design while also boosting its path loss performance. By introducing a second layer, the dispersion relation and characteristics change significantly, enabling greater freedom in design which, in turn, leads to improved performance. While the design procedure is not straightforward, the intuition behind the performance benefit is clear: since the point of maximum flux for each loop of the single-layer configuration is directly above the loop, including a second layer of loops directly above the first helps capture more magnetic flux. In turn, loss is reduced. The second layer also acts as a safeguard in case of mechanical failure: If one loop breaks, there is still a direct path for the MI waves to travel upon. Finally, the dual-layer design enables flexibility in clothing transitions, while the decreased path loss allows for larger deviations in transitions without operational failure. After optimization, this design greatly improves on the link budget (4.25 dB vs. 10.34 dB minimum path loss for the dual-layer vs. single-layer configuration), robustness to mechanical failures (16.75 dB vs. 27.31 dB minimum path loss), and the ability to transition between articles of clothing when compared to the original single-layer planar design (0.86 dB vs. 0.95 dB minimum deviation in minimum path loss). Table I summarizes the performance of the various MIW technologies, while Table II quantitatively compares the proposed dual-layer planar vs. our previously reported single-layer planar MIW [18] for a transmit distance of 41 cm under a variety of real-world scenarios that are explored in detail in Section IV.

The rest of the paper is organized as follows. Section II provides a theoretical explanation of the design as based upon a dispersion model. Section III presents a full-wave numerical analysis and experimental validation. Section IV discusses the improvements the dual-layer design offers vs. the single-layer one. Section V offers design considerations for dual-layer MIWs. Section VI discusses real-world demonstrations of the dual-layer planar MIW design. Finally, the paper concludes in Section VII.

II. THEORY OF DUAL-LAYER PLANAR MIW

A. Operating Principle

The dual-layer planar MIW is shown in Fig. 1 and consists of electrically small resonant loops placed along the direction of transmission, each separated by a gap, g. An identical layer is placed directly above the first, at a vertical distance h away from the first layer. Without loss of generality, we assume the loops to be rectangular in shape ($l \times w$) and placed upon a

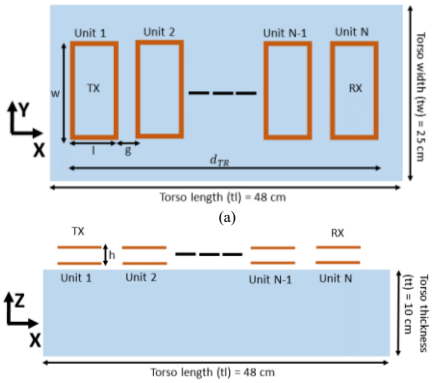

Fig. 1. Generic setup of the dual-layer planar MIW a) from a top-down view of the MIW, and b) from a side view of the MIW with the direction of propagation being in the x direction.

rectangular torso model with electrical tissue properties equal to 2/3rds that of muscle to mimic average tissue properties [20]. We include the torso model to account for the tissue loading effect but note that the impact of the permittivity of the material is negligible to the performance [19]. The operating principle is similar to that of the single-layer planar design where the transmitting (TX) loop sends MI waves towards the receiving (RX) loop through magnetic induction as mentioned in Section I. However, the major difference becomes clear when using the nearest neighbor approximation. Assuming a uniform (all loops, capacitors, and geometric gaps are identical) MIW, there is only one mutual inductance value of interest for the single-layer design (shown as M_1 in Fig. 2), while there are five mutual inductance values of interest for the dual-layer design (M, M_{1-4} in Fig. 2) [21]. While this would typically complicate the design and analysis, the number of mutual inductance values of interest can be simplified to only two values in the dual-layer case by enforcing that the top layer is identical and directly aligned with the bottom layer. With identical layers, M_1 must be equal to M_2, and through alignment, the values of $M_3$and M_4 must be equal. Since M_3 and M_4 are much smaller than both M_1 and M, they can be approximated as 0, leaving only M and M_1[21]. Here, M_1 is the mutual inductance between the two nearest loops within each layer (controlled by g) and M is the mutual inductance between the two nearest loops between each layer (controlled by h and g) as seen in Fig. 2.

B. Dispersion Model Analysis

Operation of the dual-layer planar MIW can be described through a first order dispersion model. To make the analysis possible, we assume that 1) all loops are identical, 2) all gaps g and h are identical throughout the waveguide, and 3) the waveguide is infinite in length and as such has no reflections. By utilizing the derivation in [21], which relies on the nearest neighbor approximation and symmetric simplification described above (note that the use of the symmetric simplification and nearest neighbors approximation do not

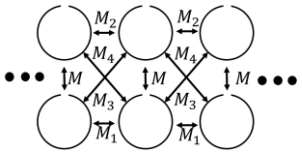

Fig. 2. Mutual inductance values for dual-layer planar MIW [21].

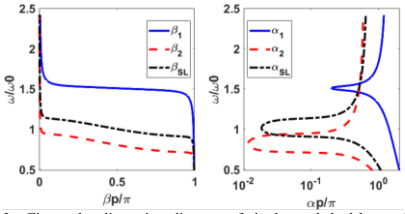

Fig. 3. First-order dispersion diagram of single- and dual-layer planar MIWs.

depend on the above assumptions), the dispersion relation is obtained as:

$$(Z + 2j\omega M_1 \cos(\gamma p))^2 = -\omega^2 M^2 \quad (1)$$

where $Z = R + j\omega L - \frac{j}{\omega C}$ is the impedance of each resonant loop (R accounts for the tissue loading effect as well as the internal resistance of the loops), $p = g + l$ is the period of the structure, and $\gamma = \beta - j\alpha$ with β as the phase constant and α as the attenuation constant.

Because the dispersion relation is quadratic in cosine of γp, there are two solutions when solving for γ, i.e., $\gamma_1 = \beta_1 - j\alpha_1$ and $\gamma_2 = \beta_2 - j\alpha_2$. Expectedly, changing any of the MIW design parameters will drastically change the dispersion behavior. Here, we select L = 260.28 nH, C = 57 pF, R = 0.85 Ω, g = 0.25 cm, l = 3.5 cm, w = 9.1 cm, and h = 0.1016 cm, which correspond to our numerical model presented in Section III, and create the dispersion diagrams in Fig. 3. For comparison, the single-layer curve from [18] is also shown (labeled as $\gamma_{SL} = \beta_{SL} - j\alpha_{SL}$).

As seen, there is a slight shift in the primary operating band away from the resonant frequency of the loops (ω_0) compared to the single-layer design. The secondary band allows for a small passband centered at approximately $1.5\omega_0$, however this passband is not of interest due to its high attenuation constant. For this example, the primary passband is centered at 34.11 MHz which is $0.825f_0$ (f_0 = 41.32 MHz) and has a bandwidth of 9.57 MHz or 28% fractional bandwidth. This theoretical bandwidth is similar to the fractional bandwidths seen in the axial design (31%) and the single-layer planar design (24%). Finally, we see that the minimum attenuation constant of γ_2 is significantly less than the minimum attenuation constant of γ_{SL}, implying improved minimum loss.

The shift in center operating frequency can be explained through a simple analysis of the dispersion relation. Starting from (1), and solving for $\cos(\gamma p)$, we attain:

$$cos(\gamma p) = \pm\frac{M}{2M_1} + j\frac{Z}{2\omega M_1} \quad (2)$$

which relates the propagation constant, γ, to angular frequency, ω, with an additional constant term related to the mutual coupling of the system. To relate this to the single-layer planar design, first we introduce a reconfigured description of the dispersion relation drawn from [18]:

$$Z + j\omega 2M_1 cos(\gamma p) = 0 \quad (3)$$

Solving (3) for $cos(\gamma p)$ with respect to ω, leads to:

$$cos(\gamma p) = j\frac{Z}{2\omega M_1} \quad (4)$$

The shift in center frequency between the single- and dual-layer designs is now clear: the ratio of the strength of the mutual coupling within the layers (M_1) and between the layers (M) leads to a variable center frequency shift due to the frequency independent term in (2) that is not present in (4).

From the dispersion diagrams, it may be reasonable to assume that attenuation can be decreased nearly indefinitely by continuously adding layers; however, this is not the case. By introducing additional layers, the MIW must be studied as a finite 2D array due to the increased interactions between each loop. These interactions do not necessarily lead to an increase in single passband performance and their study is outside the scope of this work. Additionally, while it is possible to form an MIW with more than two layers, increasing the height (thickness) of the MIW is not desirable in terms of wearability.

III. Numerical and Experimental Validation

While the dispersion diagram confirms operation under our main assumptions, an infinite length MIW is not physically possible. With MIW truncation, a frequency-dependent impedance mismatch is introduced. This mismatch can lead to significant reflections. So, despite the other assumption being maintained (identical loops and equal spacing), realizable performance can differ from theoretical performance. As such, we explore the finite length MIW numerically and experimentally to validate operation in realistic scenarios. The MIW structure is kept identical to that in Section II for comparison purposes, with the exception of two values: number of units which is truncated to 11 (for a transmit distance of 41 cm), and capacitance which is shifted to 56 pF due to commercial availability of capacitors. Note that for clarity, "loop" refers to a singular loop in the MIW while "unit" refers to the two vertically separated loops together.

As previously stated, the torso model is created using the electrical parameters equal to 2/3rds that of muscle and is set to be 50 cm × 20 cm × 7 cm. Experimentally, this is mimicked by utilizing 80% muscle / 20% fat ground beef [18, 19, 22] of the same dimensions. In both simulation and experiment, all loops are created with 30 AWG copper wire (an excellent surrogate for e-thread [23]), and the bottom layer of loops is kept a distance of 0.1 cm away from the tissue. For the experiment, loop shape and MIW structure is maintained using 3D printed molds (made from FormLabs clear resin). We note that our previous work has shown that MIW performance is invariant to underlying permittivity changes, and as such the molds should have no impact on performance [19]. The full experimental setup is shown in Fig. 4.

Ideal simulation, experimental, and shifted simulation

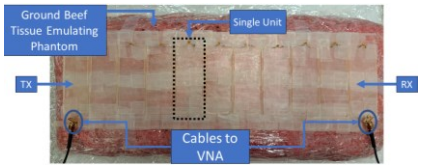

Fig. 4. Experimental setup to confirm validity of theory and numerical analysis using ground beef as the tissue phantom.

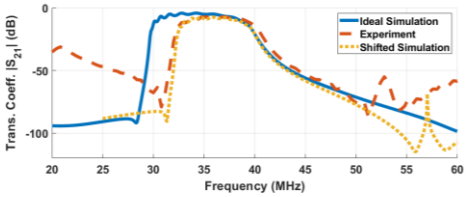

Fig. 5. $|S_{21}|$ results for the conducted experiment, an ideal simulation, and a model shifted to closely match the manufacturing defects present in the experimental setup.

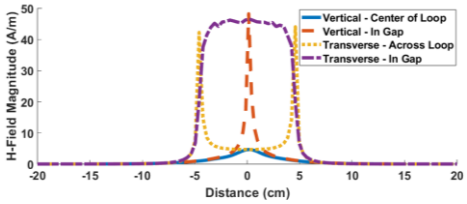

Fig. 6. Magnitude of the magnetic field at 34.4 MHz along the transverse and vertical directions with respect to MI wave propagation.

transmission coefficient ($|S_{21}|$) results are shown in Fig. 5. The simulations are created using CST Studio Suite [24]. Compared to the first-order theoretical model in Section II.B, the ideal simulation results show a slight frequency shift due to higher order interactions not quantified in the model and the slight capacitance change (centered at 34.70 MHz vs. 34.11 MHz for the theoretical model). Additionally, as with the previous MIWs studied [18, 19], there are slight ripples in the passband due to frequency-dependent impedance mismatch. The ideal MIW achieves a minimum loss of 4.25 dB at 34.24 MHz with a 10 dB absolute bandwidth of 9.44 MHz (28.1% fractional bandwidth).

The shifted simulation in Fig. 5 is an adjusted simulation used to better fit the experimental setup. This simulation increased the air gap between the layers from 0.10 cm to 0.24 cm, increased the gap between units from 0.25 cm to 0.5 cm (thereby increasing the transmit distance), and decreased the distance between the bottom layer and the tissue to 0.025 cm from 0.1 cm. It is clear from Fig. 4 and from the good agreement between the shifted and experimental results that the 3D printed molds struggled to maintain lateral and vertical distances. This issue would not be present in an e-textile implementation of the MIW due to the great precision of embroidery machines and relatively constant thickness of single pieces of clothing.

The security of the communication link is confirmed to be comparable to the single-layer planar design, with the magnetic field magnitude around the MIW being confined near to the loops along the MIW. In Fig. 6 we see the rapid decay of the magnetic field magnitude as the distance from the MIW increases in both the transverse and vertical directions at the same rate as the single-layer planar design. Additionally, anatomical curvature (e.g., arm model instead of a torso model) is confirmed to have a negligible effect on MIW performance.

IV. Demonstration of Improved Performance over Single-Layer MIWs

The following section explores the dual-layer planar MIW's improvement in robustness to mechanical failures and clothing transitions, as well as path loss versus the single-layer planar MIW. The analyses are selected to not only highlight the improvement over the single-layer design, but to also aid future designers in assessing the impact of real-world non-idealities on the desired performance. In the following, the dual-layer planar MIW is identical to the ideal simulation setup previously listed unless otherwise stated, and the single-layer planar MIW is the optimal design shared in [18].

A. Improvement in Robustness to Mechanical Failures

One flaw previously explored in the single-layer planar design is the lack of robustness in performance when a loop fails compared to the axial design [25]. While the MIW remains operational, the minimum loss drops by ~10 dB depending on which loop in the MIW is broken, compared to the 0.5-2.5 dB decrease in performance for a similar axial design. The dual-layer design greatly improves on this performance loss. For this study, we only examine a single combination of loops breaking; however, we expect these results to align with our previous work on single-layer planar and axial MIW with loop failures nearest to the TX or RX loops having a greater impact on performance than those towards the center.

When a loop is broken in the single layer case, the MIW is essentially terminated at the last loop before the break. Wireless connection can still be maintained to the remainder of the loop through magnetic induction between the previous unbroken loop and the next unbroken loop. As previously mentioned, magnetic induction falls off rapidly with distance which is why we expect a decrease in performance when a loop is broken and an even greater decrease in performance when two consecutive loops are broken. As for the dual-layer design, we expect a similar decrease in performance for full unit breaks however this design has a two-fold advantage: 1) two loops must break to completely stop the propagation of MI waves and 2) the baseline performance is improved over the single-layer design and as such a similar absolute decrease in performance between the designs will still favor the dual-layer design.

Fig. 7 shows the studied scenarios. Specifically, for the single-layer planar MIW, we examine two cases: 1) one loop breaking (loop #7), and 2) two loops breaking (loops #7 and #8). For the dual-layer planar MIW, we examine four cases: 1) one loop in unit #7 breaking, 2) one loop in unit #7 breaking and the corresponding loop in unit #8 breaking, 3) both loops in unit #7 breaking, and 4) both loops in unit #7 and #8 breaking. Note

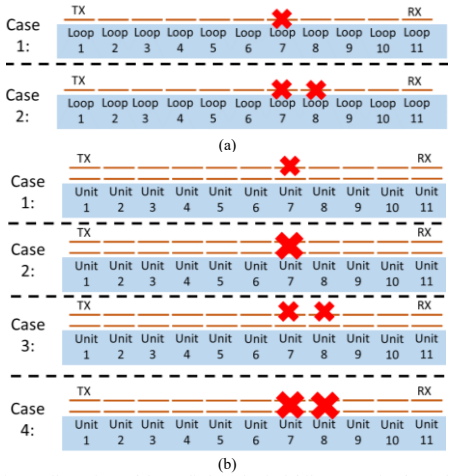

Fig. 7. Illustrations of the studied mechanical failure scenarios for a) the single-layer planar MIW and b) for the dual-layer planar MIW.

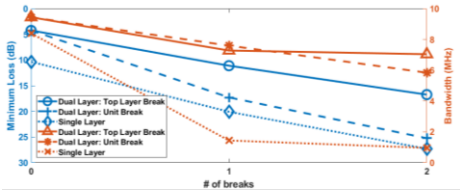

Fig. 8. Minimum loss and bandwidth with mechanical failures present in the dual-layer planar MIW and single-layer planar MIW.

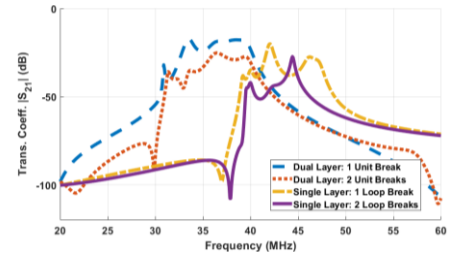

Fig. 9. $|S_{21}|$ results for various mechanical failure scenarios for the single and dual-layer planar MIW designs.

that for cases 2 and 3 of the dual-layer MIW, the results are similar if the loops that are broken are each at the top or each at the bottom, so only the case for top layer breakage is shown. The scenarios were studied via simulation as the derivation of the dispersion relation for both single- and dual- layer planar MIWs requires uniformity across the MIW and cannot handle discontinuities. In this study, loop breakage is simulated by introducing a small air gap in the loop.

Table III summarizes the minimum path loss and bandwidth results for each case, while Fig. 8 shows the change in minimum loss and bandwidth for the single- and dual-layer designs. For

TABLE III
COMPARISON OF PATH LOSS WITH MECHANICAL FAILURES

MIW	Loops Broken	Min. Path Loss (dB)	Change in Path Loss (dB)	Bandwidth (MHz)	Change in Bandwidth (MHz)
Single-Layer Planar	0	10.34	-	8.40	-
	7	20.08	9.74	1.44	-6.96
	7,8	27.31	16.97	0.96	-7.44
Dual-Layer Planar	0	4.25	-	9.44	
	7a	11.11	6.86	7.28	-2.16
	7ab	17.29	13.04	7.60	-1.84
	7a, 8a	16.75	12.50	7.04	-2.40
	7ab, 8ab	25.24	-20.99	5.84	-3.60

minimum loss, the single-layer design has the smallest change for the case of a single break. Despite this, it still has the worst minimum loss when compared to both dual-layer scenarios. Additionally, while the single-layer design minimum loss does not change under two breaks as much as the dual-layer full unit break scenario, the dual-layer design still outperforms in terms of absolute minimum loss. As for bandwidth, both dual-layer scenarios outperform the single-layer design in terms of both change in bandwidth and absolute bandwidth. Regardless of the minimum loss performance, the change in bandwidth for the single-layer design nearly eliminates the entire passband of the MIW. Finally, Fig. 9 compares the $|S_{21}|$ for the dual-layer design with full unit failures and the single-layer design with loop failures. It is clear that the passband for the single-layer design is fully eliminated with two consecutive loop failures, while the dual-layer design maintains nearly the full passband with two consecutive unit failures (four loop failures). Here, it is worth noting that loop failures are unlikely to occur due to e-threads breaking or ripping. Laboratory experience has shown that they are much more likely to fail due to issues with ceramic capacitor connections to the threads. With developments in fully textile capacitors, this issue should be mitigated [26, 27].

B. Clothing Transitions

Clothing transitions are quantified by a spatial offset between two MIWs. While in the real-world this offset can be a wide range of values in 3D space, for this study we restrict the analysis to one dimension at a time. We refer to these directions as vertical, longitudinal, and transverse as shown in Fig. 10. Per Fig. 11, four configurations are examined: 1) No overlap between the MIWs, 2) Split a unit across the article of clothing (one loop overlap), 3) one unit overlap between the MIWs, and 4) two unit overlap between the MIWs. For each configuration, the total transmit distance is kept to around 41 cm (the transmit distance will shift with transverse separation) and the loop size is $l = 3.5$ cm and $w = 9.1$ cm. For the single-layer design, the "No Overlap" and "1 Loop Overlap" cases are examined. We remark that there are four parameters of interest for clothing transition performance: 1) the maximum of the minimum path loss observed, 2) the spread in the minimum path loss, 3) the minimum bandwidth, and 4) the spread observed in the bandwidth. Here, 1) and 3) represent the worst-case performance of the communication channel under the clothing

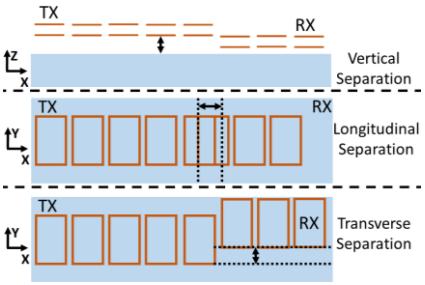

Fig. 10. Single dimension offset scenarios to model various clothing transitions for MIW use across multiple articles of clothing.

t

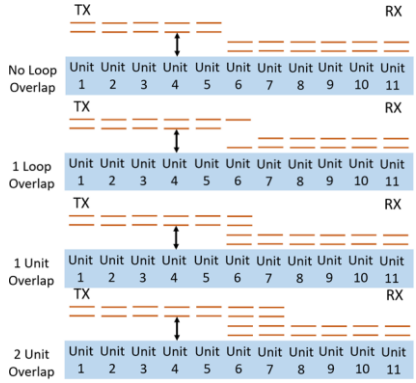

Fig. 11. Dual-layer planar configurations studied for clothing transitions.

ransition case, while 2) and 4) represent the change in communication channel characteristics. Ideally, 1), 2) and 4) are small and 3) is large.

For the purposes of WBAN application, we examine these scenarios as a single MIW with a changing discontinuity present in the chain and quantify the performance using the transmission between Unit 1 and Unit 11 as shown in Fig. 11. In general, the presented geometry can instead be examined as a 4-port network, and in particular a coupler with the additional two ports being added at the discontinuity. Creating couplers with single-layer MIWs for general application has been previously explored in [28]. A typical coupler provides an isolated port, coupled port, and through port through careful design. In this situation, we are solely interested in maximizing the transmission to the coupled port which is on the other end of the clothing transition from the input port. The following analysis numerically explores the effect of changing the mutual coupling between the MIWs on the coupled port performance for a variety of different configurations. This effect is best explored numerically due to the addition of the second layer on the dual-layer design which complicates the coupling relationship between the MIWs significantly.

1) Vertical Separation. The vertical misalignment represents the separation between articles of clothing. This value would be

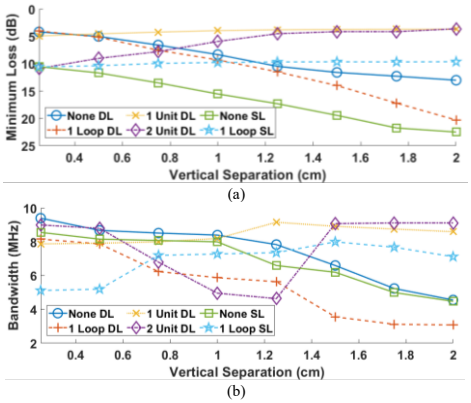

Fig. 12. Single-layer (SL) and dual-layer (DL) planar MIW configurations with changing vertical separation for a) minimum loss and b) bandwidth.

TABLE IV
COMPARISON OF PERFORMANCE FOR VERTICAL SEPARATIONS

MIW	Maximum Min. Path Loss (dB)	Min. Path Loss Spread(dB)	Minimum Bandwidth (MHz)	Bandwidth Spread (MHz)
None DL	13.01	8.84	4.56	4.84
1 Loop DL	20.30	16.28	3.08	5.08
1 Unit DL	4.91	1.23	7.88	1.28
2 Unit DL	10.86	7.25	4.64	4.48
None SL	22.50	11.97	4.48	4.08
1 Loop SL	10.58	0.95	5.12	2.88

small in thin, tight-fitting clothing and could be larger with thick and/or loose-fitting clothing. All four configurations are studied and compared to the single-layer designs in Fig. 12 for a separation distance from 0.25 to 2 cm. For the single-layer no overlap case and the dual-layer no overlap and one loop overlap cases, minimum loss monotonically increases as the vertical separation increases. On the contrary, the single-layer one loop overlap case and the dual-layer one and two unit overlap cases have a monotonic decrease in minimum loss as the vertical separation grows. Looking at bandwidth, the single-layer no overlap and the dual-layer no overlap and one loop overlap cases experience a monotonic decrease as the separations grows, while the dual-layer one unit overlap case stays relatively stable and the single-layer one loop overlap case increases. The dual-layer two unit overlap case changes sporadically.

Table IV shares the numerical results for the vertical separation. It is clear that the one unit overlap case is the most robust to vertical separations with the optimal performance in three of the four parameters vs. all other cases, including the single-layer designs. Because of the poor performance of the no and one loop overlap cases for the dual-layer design with a vertical separation, they are not considered in further results. For the further studies, the overlapping MIWs are separated by 0.5 cm.

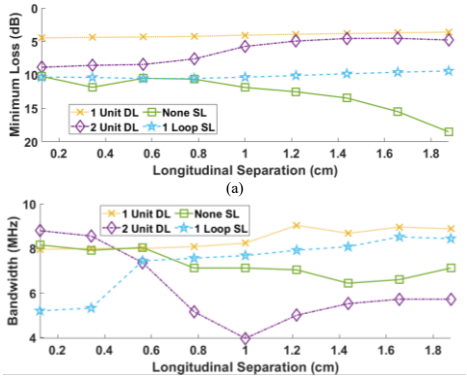

Fig. 13. Single-layer (SL) and dual-layer (DL) planar MIW configurations with changing longitudinal separation performance for a) minimum loss and b) bandwidth.

TABLE V
COMPARISON OF PERFORMANCE FOR LONGITUDINAL SEPARATIONS

MIW	Maximum Min. Path Loss (dB)	Min. Path Loss Spread(dB)	Minimum Bandwidth (MHz)	Bandwidth Spread (MHz)
1 Unit DL	4.46	0.86	7.96	1.08
2 Unit DL	8.86	4.34	3.96	4.84
None SL	18.51	8.30	6.44	1.72
1 Loop SL	10.54	1.13	5.20	3.32

DL = dual-layer, and SL = single-layer

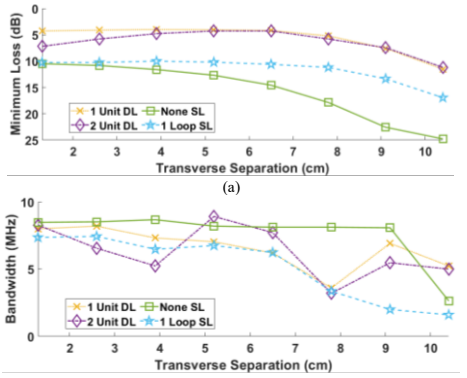

Fig. 14. Single-layer (SL) and dual-layer (DL) planar MIW configurations with changing transverse separation performance for a) minimum loss and b) bandwidth.

2) Longitudinal Separation. Longitudinal separation represents the amount of unexpected overlap between two articles of clothing. One movement that will create this type of separation is a user tilting a body part such that the MIW shifts along its transmission direction near a clothing transition e.g., tilting at the waist with an MIW spanning between the shirt and pants. The single-layer no overlap and one loop overlap, and the dual-layer one unit overlap, and two unit overlap cases are examined in Fig. 13 and Table V for longitudinal separations ranging from 0.25 cm to 1.875 cm. For both bandwidth and minimum loss, the dual-layer one unit overlap configuration is highly stable to changes in longitudinal separation making it the clear superior option for applications that may see high variance in longitudinal separation. In terms of absolute performance, the dual-layer designs outperform the single-layer designs for minimum loss. For bandwidth, the dual-layer one unit overlap design outperforms all other configurations for separations larger than 0.6 cm.

TABLE VI
COMPARISON OF PERFORMANCE FOR TRANSVERSE SEPARATIONS

MIW	Maximum Min. Path Loss (dB)	Min. Path Loss Spread(dB)	Minimum Bandwidth (MHz)	Bandwidth Spread (MHz)
1 Unit DL	11.52	7.54	3.60	4.60
2 Unit DL	11.17	6.91	3.20	5.72
None SL	24.78	14.29	2.64	6.04
1 Loop SL	16.95	6.94	1.60	5.84

DL = dual-layer, and SL = single-layer

3) Transverse Separation. Transverse separation is a shift perpendicular to the direction of propagation across the two MIWs. This type of separation would occur when a user twists their body near a clothing transition, e.g., twisting at the waist when the MIWs connect from the shirt to the pants. Fig. 14 and Table VI share the performance of the single-layer no overlap and one loop overlap, and the dual-layer one unit overlap, and two unit overlap configurations for transverse separations of 1.3 cm to 10.4 cm. For bandwidth, all four configurations have a similar performance and behavior. There is a general decreasing trend as separation increases, with some sporadic behavior throughout the range. The single-layer designs greatly underperforms vs. both dual-layer configurations in terms of minimum loss. Between the two dual-layer configurations, the one unit overlap is again the better option in terms of worst-case loss performance and change in loss performance throughout the range.

In summary, for all clothing transitions, the one unit overlap configuration for the dual-layer planar design outperforms the single-layer designs and other dual-layer design configurations in terms of loss performance. It also outperforms or performs similarly to the other dual-layer configurations in terms of bandwidth. This configuration is ideal for clothing transitions in the range of separation values tested here. While these results do not necessarily extend to larger separation values in any direction, we expect the results to extend towards multi-directional separation within the tested values. This makes the one unit overlap configuration optimal for clothing transitions for WBAN use. We also note that the one loop overlap configuration outperforms the no loop overlap for the single-layer planar design, which aligns with the dual-layer results as the one loop overlap in the single-layer case is analogous to the one unit overlap for the dual-layer case.

TABLE VII
COMPARISON OF PATH LOSS FOR MIW-WBAN TECHNOLOGIES

MIW	# of Loops	Min. Path Loss (dB)	Dual-Layer Planar MIW Improvement
Dual-Layer Planar	22	4.25	-
Single-Layer Planar	11	10.34	6.09
Axial	11	16.70	14.54
	21	9.59	7.43
	31	7.65	5.49

TABLE VIII
COMPARISON OF PERFORMANCE FOR CHANGING LOOP SHAPE

Unit Count	Loop Dimensions (l x w cm)	Min. Path Loss (dB)	Bandwidth (MHz)
5	8.00 x 4.60	4.71	5.28
7	5.64 x 6.96	6.20	8.08
8	4.90 x 7.70	3.20	9.28
9	4.33 x 8.27	3.23	10.08
11	3.50 x 9.10	3.30	11.08
15	2.50 x 10.1	4.04	12.24

C. Path Loss

Comparisons for path loss for a fixed 41 cm transmit distance are shown in Table VII. When comparing to our previous MIW designs, the dual-layer design has a path loss at least 5 dB better than the next best value, and 6 dB better than the single-layer planar design. The next best path loss occurs with an axial MIW design with a very high loop density, 31 loops in 41 cm. Due to the marginal returns seen in increasing loop density for the axial design [19], it is likely that achieving the same minimum path loss as the dual-layer planar design is not physically possible. Even if it is possible to achieve similar performance, the number of loops placed along the body may be uncomfortable to wear and would increase manufacturing costs due to increased material and complexity. Finally, we note that while not directly shown here, this improvement over our previous MIW designs also shows further improvement by up to 70 dB compared to other technologies such as RF, HBC, and MI [19].

V. DESIGN CONSIDERATIONS

For the dual-layer design, similar design analyses can be conducted as previously shown for axial and planar MIWs [19, 18]. Here, we will primarily focus on design parameters specific to a dual-layer design. The selected parameters were chosen and presented such that a designer may use the data as a guideline to help achieve the necessary performance required for specific applications.

A. Loop Shape

Because the dual-layer planar design is not limited by the underlying anatomy, the loops can take on a large number of shapes just as the single-layer design explored. By changing the loop shape while maintaining the overall electrical length, the self-inductance and mutual coupling between loops changes, thereby changing the dispersion behavior for the MIW such as the minimum loss, bandwidth and center frequency. For this study, we restrict our analyses to rectangular shaped loops based on the conclusions drawn from the single-layer design. We analyze the scenarios numerically as opposed to utilizing the theoretical dispersion relation for two reasons: 1) Particularly for the thinner loop configurations, first-order relationships are not sufficient to describe the actual behavior of the MIW as higher order coupling has a significant impact on performance and 2) The relationship between changing loop shape, self-inductance, and mutual inductance is not straight-forward and requires numerical methods to evaluate, particularly when the loops are rectangular.

The results were calculated using a dual-layer planar design with characteristics identical to the previously studied MIW (transmit distance, gap between layers, gap between units and capacitance), with two exceptions: the loop shape and therefore number of loops (the topic of study) and the underlying anatomy. This study is conducted on an arm model of radius 3.9 cm and electrical parameters of 2/3rds muscle, with the loops conformal to the arm such that the bottom layer is always 0.1 cm from the tissue and the separation distance between the layers is constant throughout. The arm model is used here without loss of generality due to the dual-layer designs invariance to underlying anatomy (discussed in Section III).

Table VIII shows the results of the loop shape analysis. There is a trend in both bandwidth and minimum loss present in the results. As the number of units increases for the same transmit distance, the bandwidth monotonically increases which is identical to what was seen in the single-layer design [18]. For the minimum loss, there is not a monotonic trend but instead an optimal value to achieve the smallest minimum loss possible. This behavior is similar to the single-layer planar design [18], however a different density is optimal to achieve the smallest loss for the dual-layer design (8 units) than the single-layer design (11 loops). For the studies presented here, we selected the 11 unit design to represent a tradeoff between loss and bandwidth and to allow for a simple extension of the previous work. We also remark that while the center frequency was shifted in the presented cases, the changes were small due to the constant electrical length of the studied loops.

B. Clearance

The vertical gap between layers (h) dubbed as the "clearance" impacts the mutual coupling between the two layers and as such can have a dramatic effect on the performance of the MIW. In particular, changing h leads to a change in M while M_1 remains unchanged. By solving (1) for $\cos(\gamma p)$ using the quadratic equation we get (5):

$$\cos(\gamma p) = j\frac{Z \pm \sqrt{Z^2 - \omega^2 M^2}}{2\omega M_1} \tag{5}$$

(5) describes the relationship between the propagation constant and M. This function is not easily analyzable due to the necessity of a complex inverse cosine hence the need to explore the situation numerically. For this study, the gap is created using air but in practice it will be created using some form of textile which has similar electrical properties to air due to the porous nature of fabric [29]. Besides the impact on performance, it is also important to keep the MIW design thin

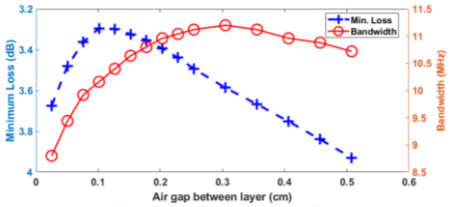

Fig. 15. Bandwidth and minimum loss results for increasing air gap between layers for the dual-layer planar MIW.

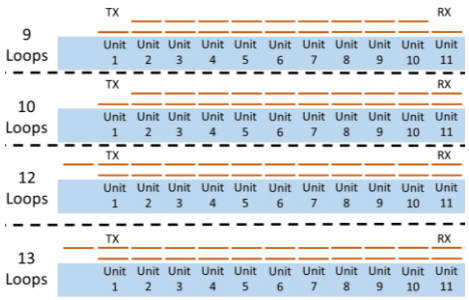

Fig. 16. Four asymmetric layer configurations explored for the dual-layer planar MIW.

TABLE IX
COMPARISON OF PERFORMANCE FOR ASYMMETRIC LAYER CONFIGURATIONS

Top Loop Count	Min. Path Loss (dB)	20 dB Bandwidth (MHz)
9	9.05	10.56
10	6.98	10.88
11	3.30	11.08
12	3.27	10.64
13	3.41	10.48

as this is a wearable design. If the design is too cumbersome, it may impede motion or cause discomfort to the user which will limit the use cases of the MIW as mentioned previously. As such we limit our scope to thickness less than ~0.5 cm.

The results are calculated using the previously described arm model and MIW configuration and are shared in Fig. 15. As the air gap distance increases, there are some small changes in minimum loss, remaining within 0.65 dB of the optimal value. The bandwidth grows rapidly as the clearance increases up to 0.30 cm. At this point, the bandwidth remains relatively constant, with a slight downward trajectory as the clearance continues to grow. For applications that require a large bandwidth, it is necessary to tradeoff between clothing thickness, and minimum loss in order to achieve the desire performance. Applications that require thin clothing should carefully control the size of the clearance as a slight variation in expected size may lead to a substantial difference in performance, particularly in bandwidth. This issue is less prevalent as the thickness is allowed to grow. For the studies shown here, an air gap of 0.10 cm was selected to minimize thickness and deliver optimal minimum loss with relatively high operating bandwidth.

We note that this analysis also serves as an example of the non-intuitive design process of the dual-layer planar design, as decreasing the coupling between the two layers by increasing the clearance leads to an enhanced performance in terms of both minimum loss and bandwidth.

C. *Asymmetric Layers*

Here, asymmetric layer design is introduced with the asymmetry surrounding the TX/RX loops. There are two main motivations for this: 1) to examine how performance is impacted by reducing the total number of loops (and therefore reducing costs) and 2) to examine if performance is impacted by increasing the total number of loops. If performance is positively impacted, the additional cost may be necessary depending on the application. Note that like the clothing transitions, this cannot be studied with the dispersion model due to the underlying assumptions of uniformity.

Five scenarios are explored through the 11-unit design placed on the previously mentioned arm model. Fig. 16 shows the asymmetric cases of interest. Throughout all scenarios, the bottom layer remains constant and the top layer changes: 1) 9 loops in the top layer (TX/RX loops do not have a secondary layer), 2) 10 loops in the top layer (One of the TX or RX loops does not have a secondary layer), 3) 11 loops in the top layer (the control), 4) 12 loops in the top layer (1 loop extends beyond the TX loop position), 5) 13 loops in the top layer (a loop extends past both TX and RX loop positions).

Table IX shows the performance of the MIW with changing top layer counts and Fig. 17 highlights the transmission characteristics. To fully capture the passbands of each design, the 20 dB absolute bandwidth is shown instead of the 10 dB absolute bandwidth (the bandwidth value shown throughout the rest of the work). One immediately obvious effect of changing the number of loops in the top layer is the change in the size of the passband ripples. As previously mentioned, these ripples are caused by reflections from a frequency dependent impedance mismatch. By reducing the overall resistance of the structure, the reflections are not absorbed as quickly which appears as larger ripples in the passband. Thus, the 9 loop design has very large ripples while the 13 loop design does not. The next immediately observable fact is that the change in loops incurs a very small change in passband size with each design being within 0.6 MHz of the ideal. Finally, the minimum loss improves in performance as the loop count increases dramatically with each loop added until the layers are symmetric, then the performance stays relatively the same, with a slight increase with 12 loops and decrease with 13 loops. The increase in performance up to 11 loops can be explained theoretically. When the first loop is excited, the direction of maximum magnetic flux is directly above the loop. This initial magnetic flux helps determine the overall performance of the MIW. With no loop placed directly above either/both the transmit and receive loops, the advantage of the dual-layer design in terms of performance is greatly reduced.

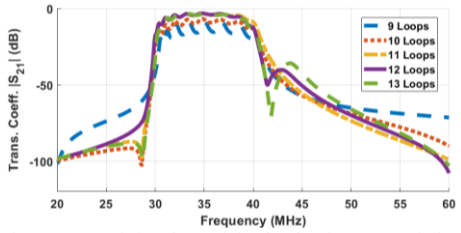

Fig. 17. Transmission characteristics for changing asymmetric layer configurations for the dual-layer planar MIW design.

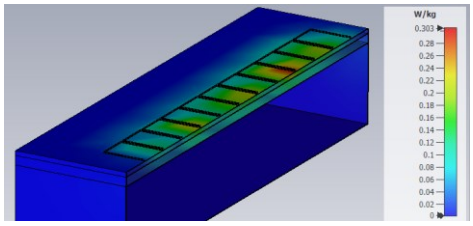

Fig. 18. 1g-averaged SAR distribution for 1 mW of input power at 34.24 MHz using a three-layer torso model.

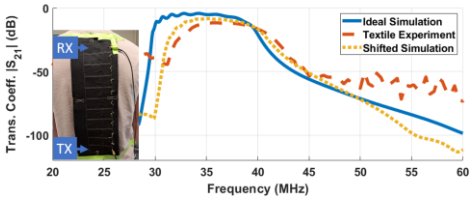

Fig. 19. Basic setup of textile MIW on a human subject and transmission characteristics of textile-based MIW, simulation, and shifted simulation.

D. *Specific Absorption Rate (SAR)*

A specific absorption rate study (SAR) is conducted to ensure that the device maintains electrical safety as define by the Federal Communications Commission (FCC) of 1.6 W/kg [30]. To represent the human body more accurately, the single-layer 2/3rds muscle model is replaced by a three-layer torso model containing 8.5 cm thick muscle, 1 cm thick fat, and 0.5 cm thick skin. The model is 48 cm long and 25 cm wide. The densities of each layer are taken from previous studies [31, 32]. The MIW design used contains 11 units, a gap of 0.25 cm, a clearance of 0.10 cm and a transmit distance of 41 cm. Fig. 18 shows the 1g averaged SAR distribution on the 3-layer torso model with a 1 mW input power. As seen, the maximum value is 0.303 W/kg which is well below the limit of 1.6 W/kg. However, it is increased from both the axial and planar designs. As we have previously shown, SAR of MIWs increases as the frequency of operation increases so this raised SAR level may impact the upper frequency limit of safe operation when compared to the axial and single-layer planar designs [19].

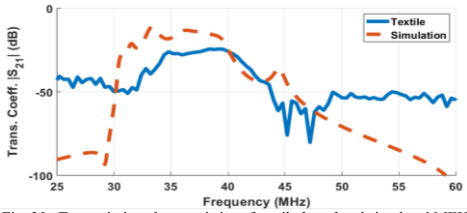

Fig. 20. Transmission characteristics of textile-based and simulated MIW with one broken loop.

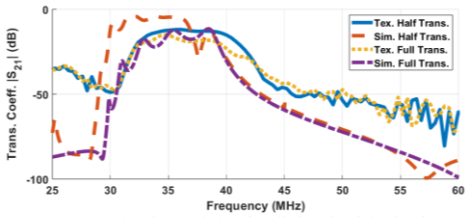

Fig. 21. Transmission characteristics of textile-based and simulated MIWs under transverse misalignment.

VI. Real-World Comparison and Case Study

In this section, we examine the application of the dual-layer planar MIW in real-world applications through experimental validation and an elaborate simulation study involving many factors previously discussed such as clothing transitions and anatomical curvature.

A. *Experimental Comparison*

Using a Brother Duetta 4500D embroidery machine and Liberator-40 conductive thread, several e-textile based dual-layer planar MIWs are constructed and tested. This fabrication technique has been used in the past for a variety of applications such as antenna design [33, 34]. The following dimensions are used to create the dual-layer planar MIW unless otherwise noted: $l = 3.5\ cm, w = 9.1\ cm,\ g = 0.25\ cm,\ h = 0.10\ cm,$ $N = 11$ (per Fig. 1). The layers of the MIW are held together using standard metal clips. The inclusion of these had a negligible effect on the experimental results.

1) Ideal Performance. The ideal performance of the dual-layer planar MIW is studied by tightly attaching the MIW on the back of a human subject, Fig. 19. Note that the location is chosen for convenience but does not impact the generality of our results. Fig. 19 shows the transmission results when compared to the simulated results shown previously, as well as a shifted simulation setup that accounts for the changed material and manufacturing limitations. The clearance is increased to 0.17 cm from 0.10 cm, the gap increased to 0.3 cm from 0.25 cm, and the conductivity of the loops reduced to 7.33×10^6 S/m (as an extrapolation of the DC resistance of the loops provided by the manufacturer). In addition, the MIW was carefully examined after fabrication and slight errors such as loop tilts and uneven gap distances were accounted for as well. As seen, there is excellent agreement between the shifted simulated and

Commented [JC1]: Do I need to make a reference for either of these?

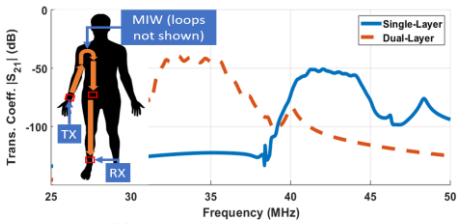

Fig. 22. Simplified setup of case study scenario and associated transmission performance for single- and dual-layer planar MIWs.

experimental results.

2) Mechanical Failures. As discussed in Section IV.A, one of the main advantages of the dual-layer planar design is the robustness to mechanical failures. To validate these results, one loop in the MIW is broken and compared to the simulated results. With the same manufacturing defects in mind as presented previously, Fig. 20 shows excellent agreement between the simulated and measured results. There is a slight frequency shift and increase in loss due to the lower conductivity of the e-thread compared to copper and other manufacturing changes as previously discussed.

3) Clothing Transitions. To experimentally compare the textile MIW with the simulated results, the transverse misalignment case is examined through half- and full-loop misalignment (4.55 cm and 9.1 cm respectively). Fig. 21 shows the comparison between the simulated and measured results for the half- and full-loop scenarios. The full transverse misalignment shows excellent agreement between the simulated and measured results. Though the half-loop case does not align as well, it does still highlight the reduction in loss and bandwidth when compared to the ideal.

B. Case Study

To further highlight the improvement over our previous work and to showcase a potential real-world application of MIW technology, a case study is conducted using both the single-layer and dual-layer planar MIWs. In this case study, we examine the hypothetical need of a researcher interested in collecting data from soccer players using body-worn sensors during real game scenarios. This application requires a data channel that can span multiple articles of clothing (to maximize athlete comfort), will maintain functionality under mechanical failures (which can occur due to the explosive nature of the sport), and can achieve high data rates. These three aspects align well with MIW use. The studied scenario analyzes implementing two sensors, placed on the wrist and ankle, one worn on the wrist, and another worn on the ankle, each communicating with one another.

The case is studied numerically by using a canonical human model with elliptical cylinders, cones, and spheres to mimic body parts. Dimensions are drawn from the average sizes of men in a large-scale study of body measurements from the United States military [35], and the model has the electrical properties equal to 2/3rds that of muscle throughout. Loops are simulated as copper wire, kept a distance of 0.1 cm away from the body model, and are conformal with the body curvature to best mimic tight-fitting clothes. Loops are built with the following values: $l = 3.5\ cm$, $w = 9.1\ cm$, $g = 0.25\ cm$, $C = 57\ pF$, and $h = 0.10\ cm$ where applicable.

We are primarily concerned with transmission along the entire body, from the wrist of the model to the ankle as that is the maximum transmission distance and ensures that all non-idealities are included in the analysis. Fig. 22 shows the transmission characteristics between the wrist and the ankle for both the single- and dual-layer planar designs. As expected, the dual-layer design has an improved minimum loss of 39.80 dB versus 50.84 dB for the single-layer planar design. This is attributed to the improvement in clothing transitions and in ideal performance. As for bandwidth, both designs achieve similar performance of 3.90 MHz and 3.96 MHz for the dual-layer and single-layer designs respectively. This is likely due to the clothing transition present in the transmission path being impacted by the conformality of the loops which may have led to a lower bandwidth than anticipated for the dual-layer design.

VII. Conclusion

In this work, we have demonstrated a dual-layer planar MIW for WBANs with large improvements in link budget, robustness to mechanical failure, and ability to handle clothing transitions vs. the state-of-the-art MIW-for-WBAN technology thereby enabling full body use. This dual-layer design also maintains the improvements vs. state-of-the-art non-MIW WBAN technologies seen in our previous MIW designs such as power requirements, interference, and security. The novelty lies on a fundamentally different theory than our previously reported single-layer MIWs, as well as the design guidelines and performance improvements presented for WBAN applications, especially as it relates to the real-world use of MIWs.

A first-order theoretical model was used to explain the operating principle and prove feasibility of the dual-layer approach. The design was validated numerically and further confirmed experimentally, with strong agreement between the results after manufacturing errors were accounted for. Improvements over the single-layer MIWs were described. The dual-layer design outperformed the single-layer planar MIW design in terms of path loss by over 6 dB and outperformed the axial MIW design by at least 5 dB, despite the increased loop density of the axial design. The dual-layer design also showed vastly improved robustness to mechanical failures vs. the single-layer planar design by being able to withstand two consecutive full unit breaks while maintaining operation. Clothing transitions were studied numerically, and the dual-layer design with a one unit overlap configuration across the transitions achieved better performance in terms of loss and bandwidth vs. the single-layer design in all scenarios. A design optimization was discussed, and SAR analysis confirmed conformance with FCC guidelines. An in-depth analysis of the real-world application of the dual-layer MIW design was conducted and confirmed the expected performance benefits presented in the idealized cases.

Future work will focus on implementing the design on full articles of clothing using conductive threads. These prototypes will enable studies examining shadowing effects, and compatibility with sensors that were not explored in this work.

REFERENCES

[1] K. Hasan, K. Biswas, K. Ahmed, N. S. Nafi and M. S. Islam, "A comprehensive review of wireless body area network," *Journal of Network and Computer Applications,* vol. 143, pp. 178-198, 2019.

[2] B. Latre, B. Braem, I. Moerman, C. Blondia and P. Demeester, "A survey on wireless body area networks," *Wireless Networks,* vol. 17, pp. 1-18, 2011.

[3] S. Movassaghi, M. Abolhasan, J. Lipman, D. Smith and A. Jamalipour, "Wireless Body Area Networks: A Survey," *IEEE Communications Surveys & Tutorials,* vol. 16, no. 3, pp. 1658-1685, 2014.

[4] M. Seyedi, B. Kibret, D. T. H. Lai and M. Faulkner, "A Survey on Intrabody Communications for Body Area Network Applications," *IEEE Transactions on Biomedial Engineering,* vol. 60, no. 8, pp. 2067-2079, 2013.

[5] R. Cavallari, F. Martelli, R. Rosini, C. Buratti and R. Verdone, "A Survey on Wireless Body Area Networks: Technologies and Design Challenges," *IEEE Communications Surveys & Tutorials,* vol. 16, no. 3, pp. 1634-1657, 2014.

[6] A. Thielens, R. Benarrouch, W. Stijn, M. Anderson, A. Moin, A. Cathelin and J. M. Rabaey, "A Comparative Study of On-Body Radio-Frequency Links in the 420 MHz-2.4 GHz Range," *Sensors,* vol. 18, no. 12, p. 4165, 2018.

[7] S. Sen, S. I. Lee, R. Jackson, R. Wang, N. Alshurafa, J. Hester and J. Gummeson, "Towards Battery-Free Body Sensor Networks," in *8th International Workshop on Energy Harvesting and Energy-Neutral Sensing Systems*, 2020.

[8] H. Baldus, S. Corroy, A. Fazzi, K. Klabunde, T. Schenk and P. Research, "Human-Centric Connectivity Enabled by Body-Coupled Communications," *IEEE Communications Magazine,* vol. 47, no. 6, pp. 172-178, 2009.

[9] D. Das, S. Maity, B. Chatterjee and S. Shen, "Enabling Covert Body Area Network using Electro-Quasistatic Human Body Communication," *Scientific Reports,* vol. 9, 2019.

[10] J. Shi and J. Wang, "Human Body Communication-Based Wearable Technology for Vital Sign Sensing," in *Wearable Technology in Medicine and Health Care*, Cambridge, Academic Press, 2018, pp. 215-233.

[11] N. Golestani and M. Moghaddam, "Theoretical Modeling and Analysis of Magnetic Induction Communication in Wireless Body Area Networks (WBANs)," *IEEE Journal of Electromagnetics, RF, and Microwaves in Medicine and Biology,* vol. 2, no. 1, pp. 48-55, 2018.

[12] F. Koshiji, Y. Fujita and K. Koshiji, "Wireless body area network using magnetically-coupled wearable coils," in *2015 IEEE CPMT Symposium Japan (ICSJ)*, Kyoto, 2015.

[13] H.-J. Kim, R. Lin, S. Achavananthadith and J. S. Ho, "Near-field-enabled Clothing for Wearable Wireless Power Transfer," in *IEEE Wireless Power Transfer Conference (WPTC)*, Seoul, 2020.

[14] R. Lin, H.-J. Kim, S. Achavananthadith, S. A. Kurt, S. Tan, H. Tao, B. C. Tee, J. K. Lee and J. S. Ho, "Wireless battery-free body sensor networks using near-field-enabled clothing," *Nature Communications,* vol. 11, pp. 1-10, 2020.

[15] A. Noda, "Wearable NFC Reader and Sensor Tag for Health Monitoring," in *IEEE Biomedical Circuits and Systems Conference (BioCAS)*, Nara, 2019.

[16] M. Wagih, "Broadband Low-Loss On-Body UHF to Millimeter-Wave Surface Wave Links Using Flexible Textile Single Wire Transmission Lines," *IEEE Open Journal of Antennas and Propagation,* vol. 3, pp. 101-111, 2021.

[17] T. T. Lan, Y. Shinozaki, T. Okura and H. Arai, "A Free-Access Segmented Coplanar Waveguide for On-Body Communication," *IEEE Transcations on Antennas and Propagation,* vol. 66, no. 9, pp. 4524-4532, 2018.

[18] V. Mishra and A. Kiourti, "Wearable Planar Magnetoinductive Waveguide: A Low-Loss Approach to WBANs," *IEEE Transactions on Antennas and Propagation,* vol. 69, no. 11, pp. 7278-7289, 2021.

[19] V. Mishra and A. Kiourti, "Wearable Magnetoinductive Waveguide for Low-Loss Wireless Body Area Networks," *IEEE Transactions on Antennas and Propagation,* vol. 69, no. 5, pp. 2864-2876, 2021.

[20] P. Soontornpipit, C. Furse and Y. C. Chung, "Design of Implantable Microstrip Antenna for Communication with Medical Implants," *IEEE Transactions on Microwave Theory and Techniques,* vol. 52, no. 8, pp. 1944-1951, 2004.

[21] O. Sydoruk, A. Radkovskaya, O. Zhuromskyy, E. Shamonina, M. Shamonin, C. Stevens, G. Faulkner, D. Edwards and L. Solymar, "Tailoring the near-field guiding properties of magnetic metamaterials with two resonant elements per unit cell," *Physical Review B,* vol. 73, no. 22, 2006.

[22] C. W. L. Lee, A. Kiourti, J. Chae and J. L. Volakis, "A high-sensitivity fully-passive wireless neurosensing system for unobtrusive brain signal monitoring," in *IEEE MTT-S International Microwave Symposium*, Phoenix, 2015.

[23] V. Mishra and A. Kiourti, "Electromagnetic Components Realized on Conductive Wires: A Copper vs. E-Thread Comparison," in *IEEE International Symposium on Antennas and Propagation and USNC-URSI Radio Science Meeting*, Atlanta, 2019.

[24] Dassault Systemes, "Electromagnetic Simulation Solvers CST Studio Suite," Simulia, [Online]. Available: https://www.3ds.com/products-services/simulia/products/cst-studio-suite/solvers/. [Accessed 29 September 2022].

[25] V. Mishra and A. Kiourit, "Wearable Magnetoinductive Waveguide WBANs: Tolerance to Loop Failures," in *2021 IEEE International Symposium on Antennas and Propagation and USNC-URSI Radio Science Meeting (APS/URSI)*, Singapore, 2022.

[26] P. Sundriyal and S. Bhattacharya, "Textile-based supercapacitors for flexible and wearable electronic applications," *Scientific Reports,* vol. 10, 2020.

[27] C. Shen, Y. Xie, B. Zhu, M. Sanghadasa, Y. Tang and L. Lin, "Wearable woven supercapacitor fabrics with high energy density and load-bearing capability," *Scientific Reports,* vol. 7, p. 14324, 2017.

[28] R. Syms, E. Shamonina and L. Solymar, "Magneto-inductive waveguide devices," *IEE Proceedings - Microwave Antennas and Propagation,* vol. 153, no. 2, pp. 111-121, 2006.

[29] R. Salvado, C. Loss, R. Goncalves and P. Pinho, "Textile Materials for the Design of Wearable Antennas: A Survey," *Sensors,* vol. 12, pp. 15841-15857, 2012.

[30] Office of Engineering and Technology, "OET - Bulletins On-Line," Federal Communications Commission, [Online]. Available: https://www.fcc.gov/general/oet-bulletins-line. [Accessed 29 September 2022].

[31] J. Kim and Y. Rahmat-Samii, "Implanted Antennas Inside a Human Body: Simulations, Designs, and Characterizations," *IEEE Transactions on Microwave Theory and Techniques,* vol. 52, no. 8, pp. 1934-1943, 2004.

[32] S. Gabriel, L. R. W and C. Gabriel, "The dielectric properties of biological tissues: II. Measurements in the frequency range 10 Hz to 20 GHz," *Physics in Medicine & Biology,* vol. 41, pp. 2251-2269, 1996.

[33] S. Alharbi, S. Chaudhari, A. Inshaar, H. Shah, C. Zou, R. Harne and A. Kiourti, "E-Textile Origami Dipole Antennas with Graded Embroidery for Adaptive RF Performance," *IEEE Antennas and Wireless Propagation Letters,* vol. 17, no. 12, 2018.

[34] A. Kiourti, C. Lee and J. L. Volakis, "Fabrication of Textile Antennas and Circuits with 0.1 mm Precision," *IEEE Antennas and Wireless Propagation Letters,* vol. 15, pp. 151-153, 2015.

[35] C. Gordon, T. Churchill, C. E. Clauser, B. Bradtmiller, J. T. McConville, I. Tebbetts and R. A. Walker, "1988 Antrhopometric Survey of U.S. Army Personnel: Summary Statistics Interim Report," United States Army Natick Research, Yellow Springs, 1989.

Connor B. Jenkins (S ’21) received the B.S. in electrical engineering from The Ohio State University, Columbus, OH, USA in 2021. He is currently continuing his education at The Ohio State University in pursuit of the Ph.D. degree under the supervision of Dr. A. Kiourti at the ElectroScience Laboratory in Columbus, OH, USA.

He has previously worked as an Engineering Education researcher at The Ohio State University where his focus was on written feedback studies. Additionally, he was an Intern with Wolfspeed Inc., (formerly Cree, Inc.) in 2020 and with Johns Hopkins Applied Physics Laboratory in 2021. His current research interests include bioelectromagnetics, electromagnetic sensors, and wearable technology.

Asimina Kiourti (S’10, M’14, SM’19) received the Diploma degree in electrical and computer engineering from the University of Patras, Patras, Greece, in 2008, the M.Sc. degree in technologies for broadband communications from University College London, London, U.K., in 2009, and the Ph.D. degree in electrical and computer engineering from the National Technical University of Athens, Athens, Greece, in 2013.

She is currently an Associate Professor at The Ohio State University Department of Electrical and Computer Engineering and the ElectroScience Laboratory, as well as an Innovation Scholar Endowed Chair at The Ohio State University College of Engineering. During her career, she has co-authored 1 book, 12 book chapters, 6 granted patents, over 75 journal papers, and over 130 conference papers and abstracts. Her research interests include bio-electromagnetics, wearable and implantable antennas, sensors for body area applications, and conductive textiles.

Dr. Kiourti has received several scholarly awards, including the 2021 NSF CAREER award, the 2021 40 Under 40 recognition by Columbus Business First, the 2018 URSI Young Scientist Award, the 2014 IEEE Engineering in Medicine and Biology Society (EMB-S) Young Investigator Award, the 2012 IEEE Microwave Theory and Techniques Society (MTT-S) Graduate Fellowship for Medical Applications, and the 2011 IEEE Antennas and Propagation Society (AP-S) Doctoral Research Award.

She is currently serving as the Senior Editor of the IEEE Open Journal of Antennas and Propagation, the Editor of the Bioelectromagnetics column of the IEEE Antennas and Propagation Magazine, and an Associate Editor for the IEEE Transactions on Antennas and Propagation, the IEEE Journal of Electromagnetics, RF and Microwaves in Medicine and Biology, and the IEEE Antennas and Propagation Magazine.